Journal of Sound and Vibration (1998) **218**(1), 65–80
Article No. sv981778

ASYMMETRIC, SPEED DEPENDENT TENSIONING OF CIRCULAR ROTATING DISKS

H. R. Kim and A. A. Renshaw

Department of Mechanical Engineering, *Columbia University*, *Mail Code* 4703, *New York*, *NY* 10027, *U.S.A.*

(*Received* 23 *February* 1998, *and in final form* 1 *June* 1998)

This paper examines the effect of asymmetry on a novel, speed dependent, in-plane stress induction technique for rotating circular disks. Residual, in-plane stresses are frequently introduced into circular saws to extend the range of stable rotation speed. The new speed dependent technique considered here is theoretically twice as effecive as traditional techniques. However, practical realization of this new technique can introduce asymmetry into the in-plane stress field, an effect that is normally not considered. In this paper, these asymmetries are explicitly examined in order to formulate design rules for the new stress induction technique. Finite element analysis indicates that at least five, evenly spaced, concentrated, in-plane loads are required along the inner radius of the disk to produce results identical to an equipollent, uniformly distributed load; four or fewer concentrated loads produce noticeably poorer results due to asymmetry. In performing these calculations, it was discovered that symmetry of the finite element mesh is essential for accurate prediction of small and vanishing natural frequencies. The viability of the new stress induction technique and the finite element predictions were both then confirmed experimentally.

1. INTRODUCTION

Residual, in-plane stresses are frequently introduced into industrial circular saws to increase certain vibration frequencies of the saw. This process, termed tensioning, increases the transverse stiffness of the saw during high speed rotation, which reduces the transverse motions of the saw caused by cutting forces. Properly tensioned saws can be thinner and can operate at higher speeds than untensioned saws, both of which increase sawmill productivity.

One well known and commonly practiced tensioning technique is *roll tensioning* [1–6]. In this technique, a thin, annular ring in the center of the saw is plastically deformed by repeatedly rolling it between two, loaded wheels. The resulting residual stresses increase the natural frequencies of those vibration modes with two or more nodal diameters, but decrease the natural frequencies of those modes with zero or one nodal diameter. If a saw is operating at a rotation speed at which the lowest natural frequency measured in the stationary frame of reference has a mode shape with two or more nodal diameters, roll tensioning will increase the transverse stiffness of the saw. This is typically the case for industrial circular saws.

0022–460X/98/460065 + 16 $30.00/0

Recently, Renshaw [7] proposed a novel tensioning strategy termed *centripetal tensioning* that is theoretically twice as effective as traditional roll tensioning. Centripetal tensioning works by having freely sliding masses rest along the inner radius of the disk while it rotates. The masses press against the inner radius of the disk with a force proportional to the square of the rotation speed, which in turn produces in-plane stresses proportional to the square of the rotation speed. Renshaw [7] showed that the benefits of tensioning are doubled when the residual stresses are speed dependent in this manner rather than permanent, as they are in traditional tensioning techniques.

In practice, however, the uniformly distributed masses used in describing centripetal tensioning are a finite number of massive wedges resting against the inner radius of the disk. Under ideal conditions, these wedges make full contact with the inner radius of the disk over the complete arc of the wedge and produce a contact pressure that is nearly uniform. However, since these wedges must be able to move freely in the plane of the disk, it is possible, and perhaps even likely, that the wedges will become cockeyed, in which case the contact pressure from each wedge may approximate a concentrated load rather than a uniform pressure. Under these conditions, the in-plane stress field in the disk will no longer be axisymmetric and the benefits of centripetal tensioning will be reduced. The design question then arises: how many wedges are required to achieve the benefits of centripetal tensioning under the worst possible asymmetry?

Disk-based asymmetries in either the stress or geometry of a rotating disk complicate the analysis of its response to stationary transverse loads since the rotating asymmetries preclude a simple frequency analysis in the stationary frame of reference. As a result, prior research on disk-based asymmetries has focused almost exclusively on stationary disks. An exception is Mote [8] who developed a finite element for the analysis of a slotted rotating plate by analyzing the disk in the rotating frame of reference. More typically, Parker and Mote [9] examined asymmetric tensioning in a stationary disk using the finite element method and concluded that, in contrast to axisymmetric tensioning, all natural frequencies of the disk could be increased by asymmetric stress fields. Yu and Mote [10] and Shen and Mote [11–13] calculated the parametric resonance of asymmetric disks subjected to rotating springs. Chen and Jhu [14] examined a spinning disk subjected to a stationary edge load, which produces an asymmetric but non-rotating stress field in the disk.

In this paper, finite element analysis is used to calculate the stress field and natural frequencies of a rotating disk in the rotating frame of reference when the inner radius of the disk is subjected to a series of evenly spaced, concentrated, in-plane, speed dependent loads. These calculations indicate that at least five concentrated loads are needed to fully achieve the benefits of centripetal tensioning, with four or fewer concentrated loads being significantly less effective. In performing these calculations, it was discovered that symmetry of the finite element mesh is essential for accurate prediction of small and vanishing natural frequencies. The accuracy of these predictions and the viability of centripetal tensioning were then confirmed in a series of centripetal tensioning experiments. This corroboration demonstrates that substantial improvements in tensioning

practice can be achieved using speed dependent tensioning techniques. These new techniques may lead to a new generation of circular saws with considerably higher levels of performance than the existing generation of circular saws.

2. MATHEMATICAL MODELLING

A thin, axisymmetric, circular disk is transversely clamped at inner radius R_i and free at outer radius R_o. The disk is of uniform thickness h, Young's modulus E, density ρ (mass per unit volume), and Poisson's ratio ν, and spins about its axis of symmetry at a constant angular speed Ω^*. $W(T, R, \theta)$ is the transverse displacement of the disk where T is time and polar co-ordinates (R, θ) are fixed on the rotating disk with the center of the disk at the origin. The in-plane, axisymmetric stresses σ_r^*, σ_θ^*, and $\tau_{r\theta}^*$ are measured in the rotating frame of reference. The equation of motion in the *rotating* frame of reference derived from Kirchhoff plate theory with in-plane stress is [15].

$$\rho h W_{,TT} - h(R\sigma_R^* W_{,R} + \tau_{R\theta}^* W_{,\theta})_{,R}/R - h(\tau_{R\theta}^* W_{,R} + \sigma_\theta^* W_{,\theta}/R)_{,\theta}/R + D\nabla^4 W = 0, \tag{1}$$

where ∇^4 is the biharmonic operator, a comma indicates partial differentiation, and $D = Eh^3/12(1 - \nu^2)$.

Dimensionless variables are defined by

$$r = R/R_o, \qquad w = W/h, \qquad t = T\sqrt{D/\rho h R_o^4}, \qquad \Omega = \Omega^*\sqrt{\rho h R_o^4/D},$$
$$\sigma_r = \sigma_r^* h R_o^2/D, \qquad \sigma_\theta = \sigma_\theta^* h R_o^2/D, \qquad \tau_{r\theta} = \tau_{r\theta}^* h R_o^2/D. \tag{2}$$

The clamping ratio is $\kappa = R_i/R_o$. Under definitions (2), equation (1) becomes

$$w_{,tt} - (r\sigma_r w_{,r} + \tau_{r\theta} w_{,\theta})_{,r}/r - (\tau_{r\theta} w_{,r} + \sigma_\theta w_{,\theta}/r)_{,\theta}/r + \nabla^4 w = 0, \tag{3}$$

where ∇^4 has been re-defined in terms of r instead of R. w satisfies clamped–free boundary conditions

$$w = 0 \quad \text{and} \quad w_{,r} = 0 \quad \text{at} \quad r = \kappa,$$
$$w_{,rr} + \nu(w_{,r}/r + w_{,\theta\theta}/r^2) = 0 \quad \text{at} \quad r = 1,$$
$$(\nabla^2 w)_{,r} + (1 - \nu)(w_{,r\theta\theta}/r^2 - w_{,\theta\theta}/r^3) = 0 \quad \text{at} \quad r = 1, \tag{4}$$

where ∇^2 is the Laplacian. The substitution

$$w(t, r, \theta) = \mathrm{e}^{\mathrm{i}\omega t} u(r, \theta), \tag{5}$$

where $\mathrm{i} = \sqrt{-1}$, converts equation (3) into the eigenvalue equation

$$-\omega^2 u - (r\sigma_r u_{,r} + \tau_{r\theta} u_{,\theta})_{,r}/r - (\sigma_\theta u_{,\theta}/r + \tau_{r\theta} u_{,r})_{,\theta}/r + \nabla^4 u = 0, \tag{6}$$

where ω is the natural frequency in the rotating frame of reference.

The stresses satisfy the plane stress equilibrium equations of linear elasticity:

$$\sigma_{r,r} + (\sigma_r - \sigma_\theta)/r + \tau_{r\theta,\theta}/r = -\Omega^2 r, \tag{7}$$

$$\sigma_{\theta,\theta}/r + \tau_{r\theta,r} + 2\tau_{r\theta}/r = 0, \tag{8}$$

subject to the boundary conditions

$$\sigma_r = \sigma_r^o(\theta) \quad \text{and} \quad \tau_{r\theta} = \tau_{r\theta}^o(\theta) \quad \text{at} \quad r = \kappa, \tag{9}$$

$$\sigma_r = \tau_{r\theta} = 0 \quad \text{at} \quad r = 1. \tag{10}$$

Since the solutions of equations (7) and (8) decouple from equation (6), they can be solved first for σ_r, σ_θ, and $\tau_{r\theta}$ and then these solutions can be plugged into equation (6) as known functions during the determination of ω and $u(r)$.

For ideal centripetal tensioning, the stress boundary conditions (9) are the axisymmetric conditions [7]

$$\sigma_r = -m\Omega^2 \quad \text{and} \quad \tau_{r\theta} = 0 \quad \text{at} \quad r = \kappa, \tag{11}$$

where m is a fixed constant that represents dimensionless added mass, assumed to be concentrated in a line around the inner radius $r = \kappa$. $m = 0$ represents an annular disk with no traction at $r = \kappa$ which is often used to model rotating disk systems [16].

The equations governing the motion of the disk in the *stationary* frame of reference can be derived by transforming w, σ_r, σ_θ, $\tau_{r\theta}$, and equations (3), (4), and (7)–(10) using the transformation [17]

$$\theta' = \theta - \Omega t. \tag{12}$$

In the special case in which the stresses are axisymmetric (i.e., $\sigma_r = \sigma_r(r)$, $\sigma_\theta = \sigma_\theta(r)$, $\tau_{r\theta} = 0$), the resulting equation of motion is autonomous in time, and the natural frequencies in the stationary frame of reference can be found using an harmonic substitution similar to equation (5). In this special case, the eigenvalue problem in either frame of reference is separable in θ and the mode shapes have the form

$$u(r, \theta) = \mathrm{e}^{\mathrm{i}n\theta} f_n(r), \tag{13}$$

where $n = 0, \pm 1, \pm 2, \ldots$ is the number of nodal diameters in the mode shape. A straightforward calculation shows that the natural frequencies in the stationary frame of reference, λ, are related to the natural frequencies in the rotating frame of reference, ω, by the relation

$$\lambda = \omega \pm n\Omega. \tag{14}$$

Those eigensolutions with the plus sign in equation (14) are associated with circumferentially travelling wave solutions that move in the direction of rotation, which are normally termed forward wave solutions, whereas those associated with the minus sign in equation (14) are termed backward travelling wave solutions.

Figure 1 compares the natural frequencies of a typical, axisymmetric, rotating disk with $\kappa = 0{\cdot}3$ in both the rotating and stationary frames of reference. These frequencies were calculated using the Galerkin method with ten orthonormal, Chebyshev polynomials defining the separable, radial part of the eigenfunctions. In the rotating frame of reference, all natural frequencies except $n = 0$ are repeated and all frequencies increase as Ω increases due to the tensile centripetal stresses in the disk. However, in the stationary frame of reference, the natural frequencies

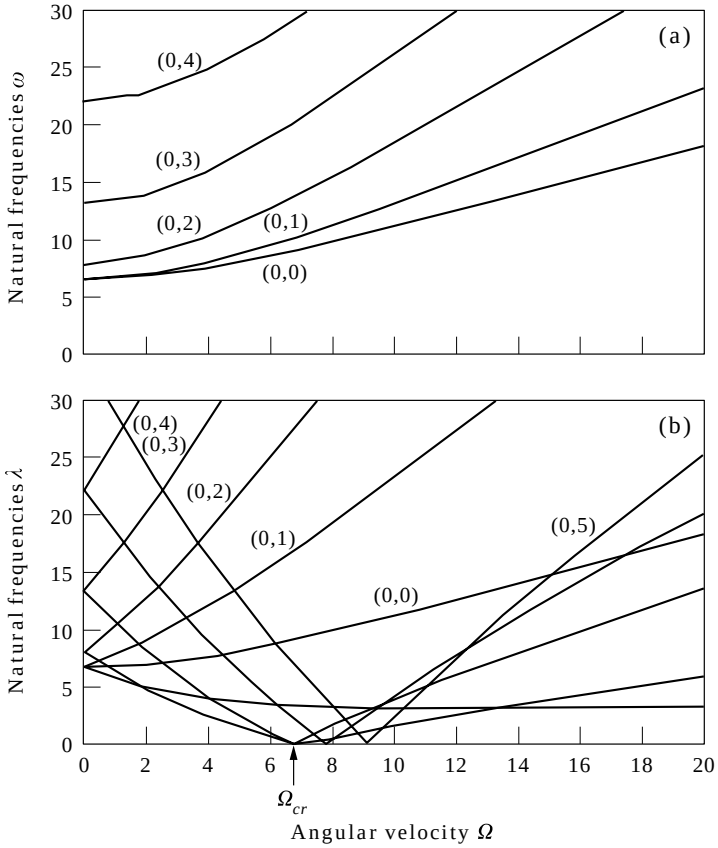

Figure 1. Natural frequencies of a typical, axisymmetric, rotating disk with $\kappa = 0{\cdot}3$ in (a) the rotating frame of reference, and (b) the stationary frame of reference. (i, j) modes denote i nodal circles and j nodal diameters.

associated with backward travelling waves initially decrease as Ω increases (except for $n = 0$ which does not decompose into forward and backward wave solutions) and can become quite small. These small magnitude natural frequencies can lead to significant vibration in rotating disk systems. The critical speed Ω_{cr} is defined as the lowest angular velocity at which a backward natural frequency vanishes. This is often the upper limit of rotation speed for rotating disk systems since the disk can be resonated by stationary loads at that speed. For $\kappa = v = 0{\cdot}3$, $\Omega_{cr} = 6{\cdot}6$ and the vibration mode whose frequency vanishes at this speed has three nodal diameters.

When the stresses are asymmetric and fixed on the rotating disk, the transformation (12) produces an equation of motion with periodic coefficients, e.g., the rotating stress fields. Consequently, the natural frequencies in the stationary frame of reference cannot be calculated using a simple harmonic substitution. The response and stability of *stationary*, asymmetric systems subjected to moving loads has been predicted using parametric excitation analysis by several researchers [10–13]. In the present case, a rigorous parametric analysis could be done for the asymmetric, *rotating* disk subject to a load moving at a

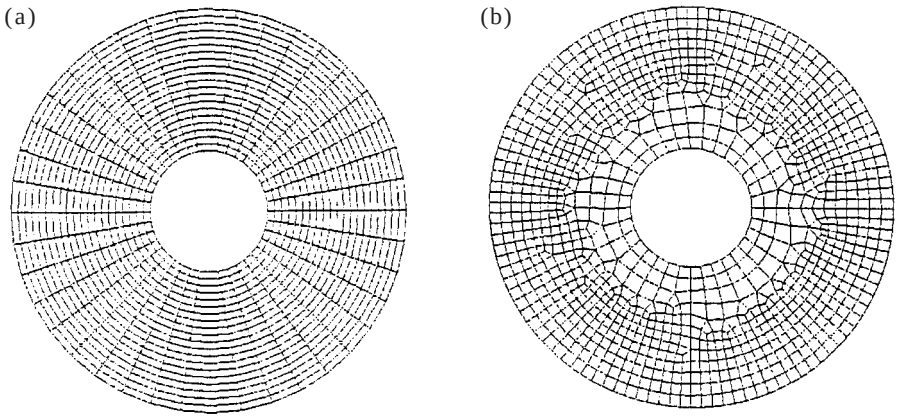

Figure 2. Sample meshes used in the finite element convergence study: (a) a symmetric mesh; (b) an asymmetric mesh.

constant speed relative to the rotating disk to determine the speeds at which resonance occurs. (The disk cannot be stationary since the asymmetric stresses are generated only during rotation.) However, such an analysis and the development of appropriate computational tools exceeds the scope of the present paper. Instead, we seek a plausible analytical approach using existing computational tools that will permit us to formulate design rules that can be verified experimentally.

TABLE 1

Natural frequencies for an axisymmetric disk with and without mesh symmetry

	Number of elements					
Symmetric	72	288	648	1056	Galerkin prediction	Percentage error
Mode						
(0,0)	0·4781	1·8551	2·1318	2·2588	2·3647	−4·48
(0,1)	13·2719	13·4771	13·5130	13·5169	13·5352	−0·14
(0,1)	13·2719	13·4771	13·5130	13·5169	13·5352	−0·14
(0,2)	24·6793	25·8315	26·0525	26·1153	26·2295	−0·44
(0,2)	24·6802	25·8318	26·0525	26·1153	26·2295	−0·44
	Number of elements					
Asymmetric	52	265	729	1029	Galerkin prediction	Percentage error
Mode						
(0,0)	5·2279	3·6546	1·2716	0·2074	2·3647	−91·23
(0,1)	13·4579	13·6831	13·5946	13·5877	13·5352	0·39
(0,1)	13·4996	13·7233	13·6057	13·5890	13·5352	0·40
(0,2)	24·2087	25·8161	26·0813	26·1278	26·2295	−0·39
(0,2)	24·2634	25·8279	26·0864	26·1294	26·2295	−0·38

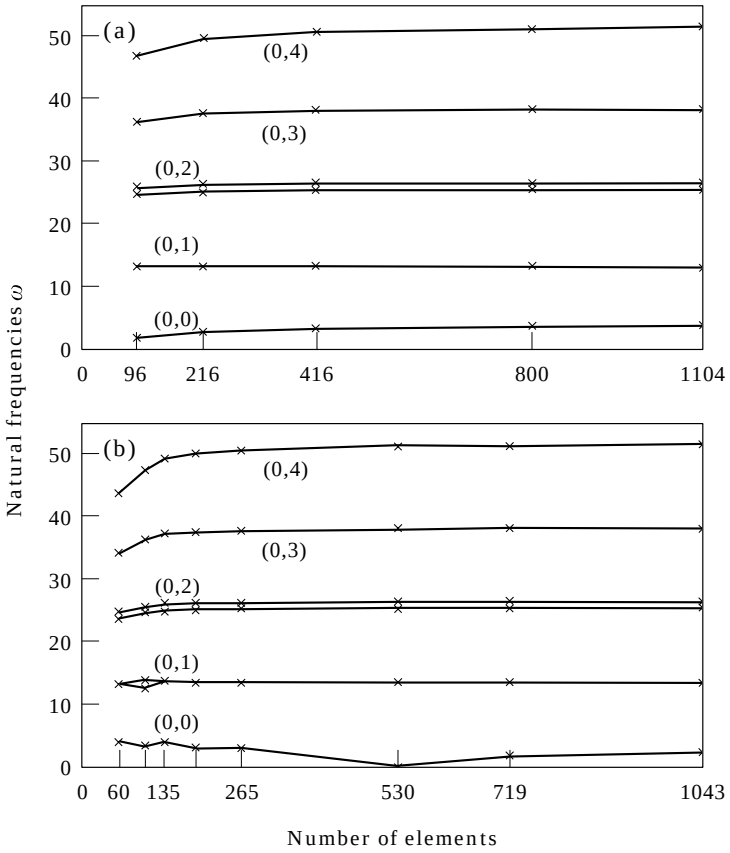

Figure 3. Finite element convergence results for (a) symmetric and (b) asymmetric meshes using four concentrated point loads along the inner edge of the disk.

A common rule of thumb for simplifying the analysis of rotating asymmetric disks is to assume *a priori* that increases in natural frequency in the rotating frame of reference reduce the transverse vibrations of the disk caused by stationary loads [8, 9]. Although not rigorous, we adopt this *ad hoc* strategy here for reasons of simplicity and practicality and define the frequency margin

$$FM = \omega - n\Omega \tag{15}$$

as a means of comparing the vibration frequencies of the disk with asymmetric stress in the rotating frame of reference to those of an axisymmetric disk in the stationary frame of reference. In the case of axisymmetric stresses, FM equals the frequency of the backward travelling waves. In computing equation (15), n is half the number of nodal lines extending from $r = \kappa$ to $r = 1$. Because of the asymmetry, these may no longer lie along radii of the disk. According to our *ad hoc* design rule, FM should be as large as possible to reduce disk vibration. Vanishing FM may indicate particularly high sensitivity to transverse loads since FM vanishes at the critical speeds of an axisymmetric disk.

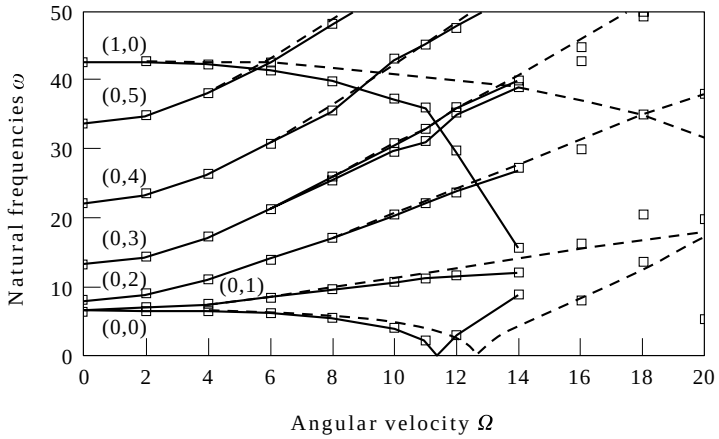

Figure 4. Natural frequencies in the rotating frame of reference as a function of Ω for $p = 3$ concentrated point loads (squares interpolated with the solid line) compared with the axisymmetric $p \to \infty$ frequencies (dashed line).

3. ASYMMETRIC SPEED DEPENDENT TENSIONING

We wish to consider the case where the axisymmetric inner boundary condition for speed dependent tensioning (equation (11)) is replaced by a set of p evenly spaced, equipollent, concentrated loads, e.g.,

$$\tau_{r\theta} = 0 \quad \text{and} \quad \sigma_r = -\frac{2\pi m\Omega^2}{p}\,\delta(\theta - 2\pi j/p) \quad \text{at} \quad r = \kappa, \quad j = 0, 1, \ldots, p-1, \tag{16}$$

where $\delta(\,\cdot\,)$ is the Dirac delta function. These boundary conditions simulate the worst case asymmetry in the physical realization of equation (11) which occurs when all wedges become sufficiently cockeyed that they make contact with the disk only along a sharp edge. As $p \to \infty$, the axisymmetric boundary condition (11) is recovered. It is assumed that more axisymmetric loading (e.g., when the wedges

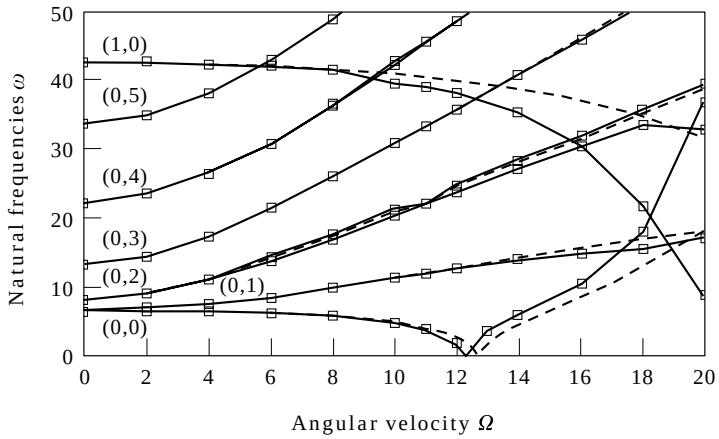

Figure 5. Same as Figure 4 with $p = 4$.

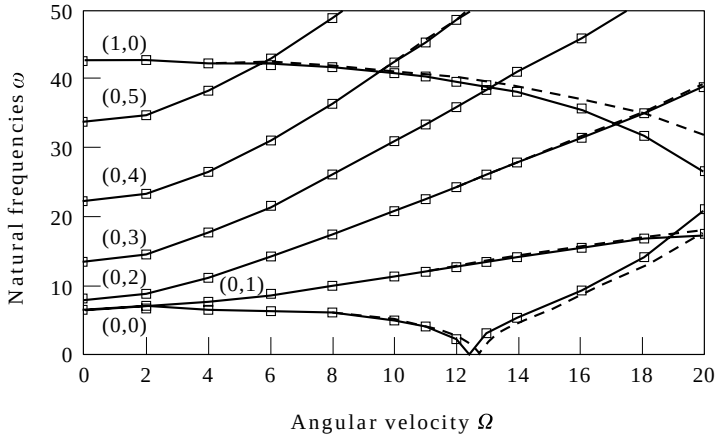

Figure 6. Same as Figure 4 with $p = 5$.

are flush with the disk over complete sectors) will produce tensioning results that are as good, if not better, than this worst case scenario.

We used SDRC's I-deas finite element program to mesh and solve these problems with bilinear, quadrilateral elements using the Lanczos algorithm. Convergence studies were performed using two kinds of meshes: a mapped mesh with a regular pattern of symmetric elements, and a "free mesh", in which the computer automatically fills the mesh area with an asymmetric pattern of elements. Examples of symmetric and asymmetric meshes are shown in Figure 2. The problem used for the convergence study was the axisymmetric centripetal tensioning problem defined by equation (1) with $m = 1{\cdot}33$, $\kappa = 0{\cdot}3$, and $\Omega = 13$. These conditions represent almost optimum centripetal tensioning and are characterized by a small magnitude (0,0) natural frequency where (i, j) indicates modes with i nodal circles and j nodal diameters. (The circles and diameters may

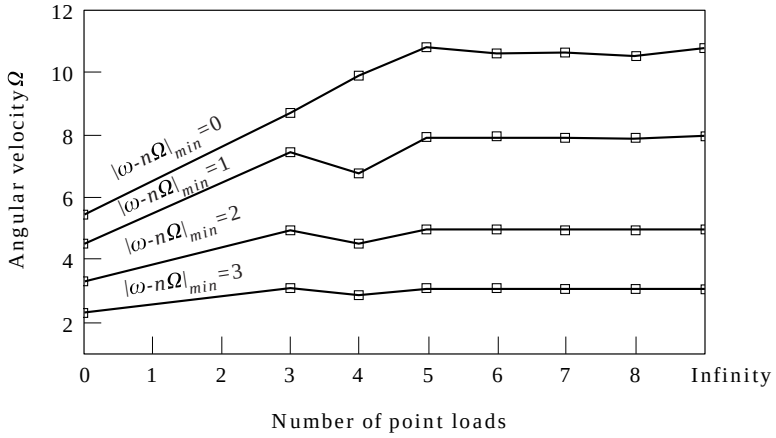

Figure 7. The angular speed at which $FM = 0, 1, 2$, and 3 as a function of p. $p \to \infty$ represents the axisymmetric results for which FM represents a natural frequency.

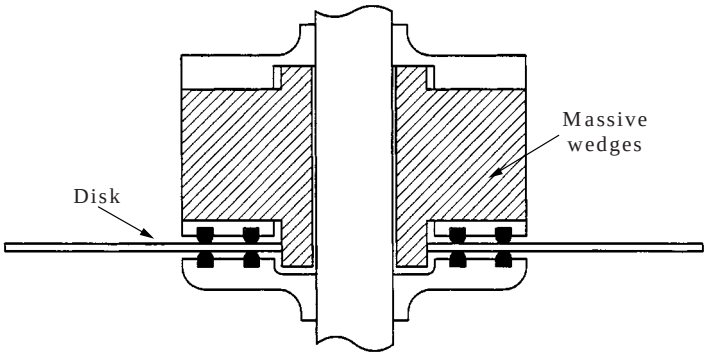

Figure 8. A schematic of the centripetal clamp design.

be imperfect when asymmetric stresses are present.) The results of this convergence study are shown in Table 1.

In most cases, the finite element natural frequencies converge to the values predicted using Galerkin's method as the number of elements increases, and is generally within a few percent of that value once there are more than about 500 elements. The single exception to this is the finite element prediction of the (0,0) natural frequency using the asymmetric mesh. The predicted frequency does not appear to converge as the number of elements increases and occasionally is very close to vanishing. The vanishing of this frequency is an important parameter because it limits the tensioning technique, and its prediction is crucial to this analysis. Note that with the symmetric mesh there is no convergence problem.

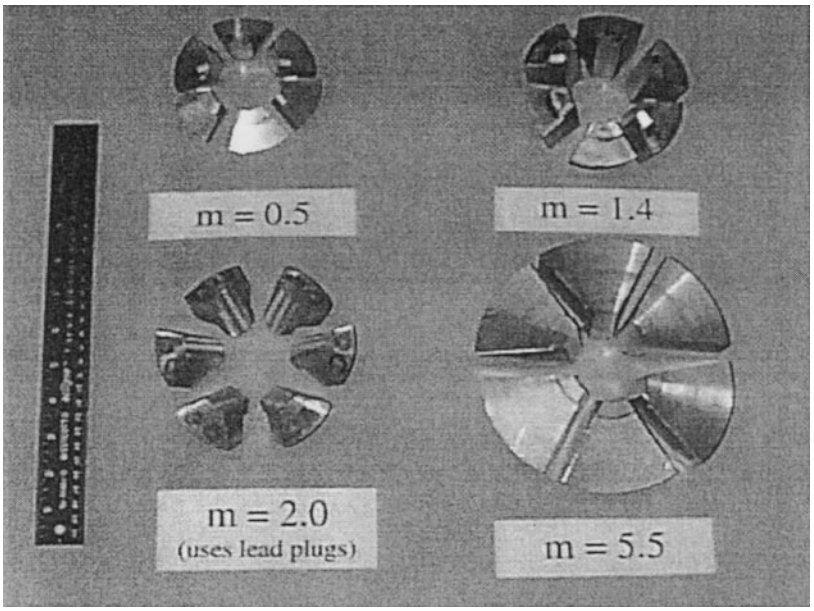

Figure 9. Different size wedges used to achieve $m = 0{\cdot}5$, $1{\cdot}4$, $2{\cdot}0$, and $5{\cdot}5$. A 12″ ruler is shown on the left.

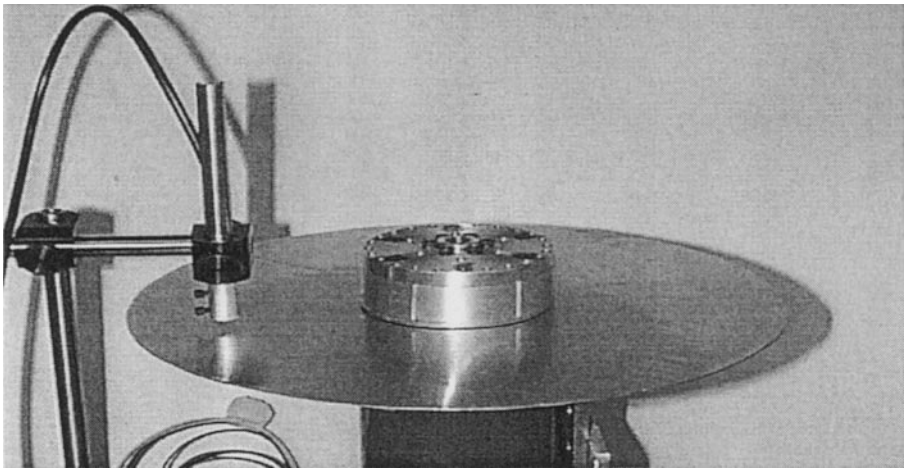

Figure 10. The centripetal clamp experimental set-up with $m = 2{\cdot}0$.

Furthermore, the *only* difference in the results is the mesh since the same code is used in both cases.

Note also that even though the disk is axisymmetric, two vibration frequencies are listed for the (0,1) and (0,2) modes in each case even though it is known that these vibration frequencies are repeated. The finite element predictions of these frequencies will only be repreated if the discretization possesses the same axisymmetry as the disk. Even for the symmetric mesh, the finite element results do not possess perfect axisymmetry since a rotation of half an element width does not give the same discretization. However, this effect is small. For the symmetric mesh, the frequencies are the same for 648 and 1056 elements. The error in the other two cases is less than 0·004%. The discrepancies for the asymmetric mesh are, of course, larger since this mesh is not axisymmetric at all, but the discrepancies are still less than 1%.

Meshing problems can also occur when the stresses in the rotating disk are not symmetric. Figure 3 shows the natural frequencies of the same centripetal tensioning problem except with equation (11) replaced by equation (16) with $p = 4$. Although there is no simple Galerkin solution with which to compare these results, all frequencies appear to converge except the (0,0) mode frequency using the asymmetric mesh. In fact, the asymmetric mesh results predict disk buckling at 530 elements. Note also that the (0,2) mode has split into two distinct frequencies in both meshes due to the asymmetric stress. (The effects of asymmetry could be analyzed using a standard eigenvalue perturbation approach if the stress problem could be easily decomposed into a symmetric problem with a small perturbation [10]. Such an approach was not pursued here.)

Perkins and Mote [18] observed that discretizations such as finite element meshes that did not preserve the geometric symmetry of a problem sometimes produced spurious frequency results. A similar effect appears to occur in this problem for small magnitude frequencies of a rotating disk. These frequencies do not appear to converge properly in the finite element method as the number of

elements increases unless the elements are symmetric. Subsequent results in this paper were all generated using symmetric meshes.

Figures 4–6 show the natural frequencies predicted by the finite element method for asymmetric boundary conditions (16) with $p = 3$, 4, and 5 compared with the axisymmetric natural frequencies.

For $p = 3$ (Figure 4), there are significant frequency deviations for the (0,0), (0,1), and (1,0) modes and modest deviations for the other modes. However, modest differences in natural frequency in the rotating frame of reference can produce substantial differences in FM when $n \neq 0$. For example, for the (0,3) mode at $\Omega = 10$, $\omega = 29{\cdot}7$ when $p = 3$ as compared to $\omega = 30{\cdot}9$ under axisymmetric boundary conditions (11), which is only a 3·9% difference. The associated frequency margins computed using equation (15) are $FM = -0{\cdot}3$ and $FM = 0{\cdot}9$ which represent a 400% difference and have dramatically different stability implications.

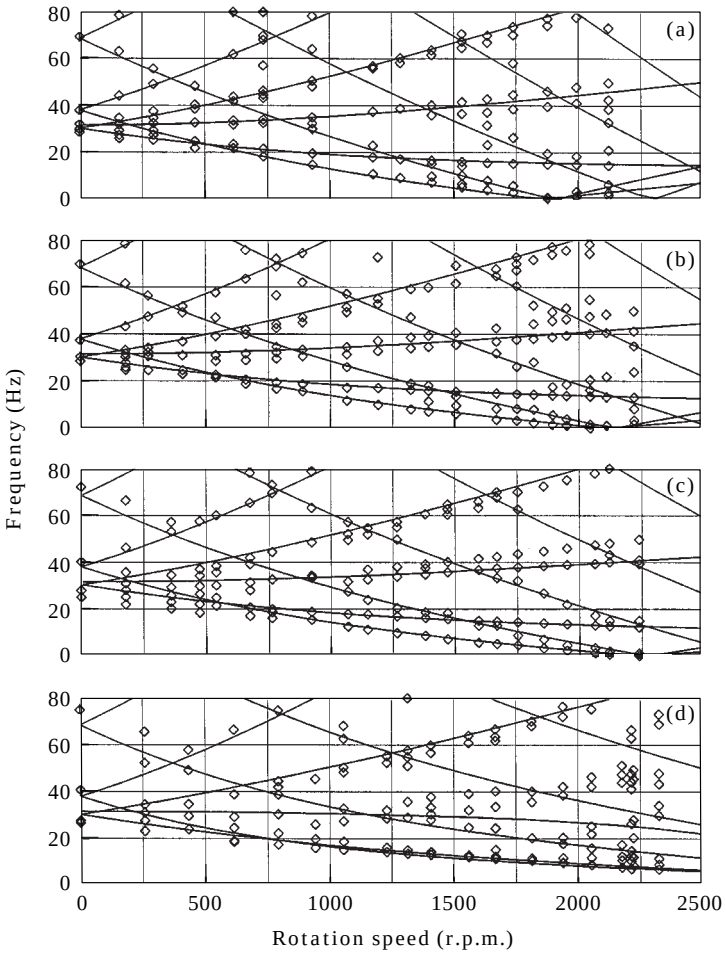

Figure 11. Experimentally measured (diamonds) and theoretically predicted (solid lines) natural frequencies in the stationary frame of reference as functions of rotation speed for: (a) $m = 0$; (b) $m = 1{\cdot}4$; (c) $m = 2{\cdot}0$; and (d) $m = 5{\cdot}5$.

TABLE 2

Comparison of theoretical and experimental critical speeds from the data in Figure 11. *The critical speed for* $m = 5.5$ *was too high to be measured with the set up described*

m	Predicted critical speed (r.p.m.)	Measured critical speed (r.p.m.)	Percentage error
0	1861	1862	0·1
1·4	2111	2044	3·2
2·0	2252	2238	0·6
5·5	3079	>2400	–

For $\Omega > 14$, the finite element data is shown but not interpolated because the asymmetry is so great that it is difficult to distinguish and somewhat arbitrary to assign the (0,0), (0,1), and (1,0) modes to a particular frequency. The natural frequencies were also calculated for $p = 2$, but the asymmetry in the stresses was so large for this case the natural frequencies were not even worth comparing to the axisymmetric case. It suffices to say that these results are not comparable to axisymmetric tensioning.

The case $p = 4$ (Figure 5) shows significant frequency variations in the (0,0), (0,1), and (1,0) modes and modest variations in the other modes, but these variations are less than they are for $p = 3$. For the (0,2) mode, ω splits into two distinct frequencies because of the asymmetry of the stress [10]. This split is so large that the frequency margin of the (0,2) mode vanishes before the (0,3) mode. This is the opposite of what happens in axisymmetric tensioning.

The results for $p = 5$ (Figure 6) are essentially identical to the axisymmetric case for $\Omega < 13$. There are variations in the (0,0) and (1,0) modes, but the frequency margins for these modes are still very close to the axisymmetric predictions. Additional calculations for $p = 6$, 7, and 8 showed even less differences with the axisymmetric predictions.

The angular speed at which the minimum FM among all vibration modes first equals 0, 1, 2, and 3 is shown as a function of p in Figure 7. This graph can be used to summarize the effect of asymmetric tensioning by comparing the asymmetric results (finite p) to the axisymmetric results ($p = \infty$). For the crucial case where the frequency margin first vanishes, $p \geqslant 5$ in order to produce results identical to the axisymmetric case. For $p = 3$ and 4, the speed at which FM vanishes is 23·0% ($\Omega = 9{\cdot}7$) and 13·5% ($\Omega = 10{\cdot}9$) below the speed at which axisymmetric stresses produce vanishing FM ($\Omega = 12{\cdot}6$). This is also true for $FM = 1$, but for $FM = 2$ and 3, p can be somewhat smaller without significantly altering the speed at which the frequency margin is achieved. For $FM = 2$ and 3, however, the relative increase in natural frequency from the case where no tensioning is applied ($p = 0$) is small. In these cases, the benefits of centripetal tensioning may be marginal.

In summary, therefore, for devices that operate at a large fraction of critical speed, i.e., near $FM = 0$, no fewer than five wedges are recommended as a general design rule when centripetal tensioning is used.

4. EXPERIMENTAL RESULTS

The design guidelines developed in the previous section as well as the practical viability of centripetal tensioning were verified in a series of experiments. A 30-cm diameter, 0·5-mm thick, aluminum disk was attached to a brushless DC motor using a special clamp designed to produce centripetal clamping results for different values of m. A schematic of the clamp is shown in Figure 8. The disk is supported between two O-rings that control the transverse position of the disk while allowing it to expand radially. A set of six massive wedges are inserted into the clamp so that a tab at one end of the wedge lies between the shaft of the motor and the inner edge of the disk. A tab on the other end of the wedge is supported by the other end of the clamp. During rotation, each of the six wedges is flung outwards with a force proportional to the square of the rotation speed, and that load is divided between the two tabs on each wedge. Thus, the inner edge of the disk experiences a speed dependent load during rotation. Different tension magnitudes m were achieved using different size wedges. Figure 9 shows the wedges used to achieve centripetal clamping with $m = 0{\cdot}5$, 1·4, 2·0, and 5·5. Figure 10 shows the experimental set-up with the $m = 2{\cdot}0$ wedges in place. The central hole of the disk was 5 cm in diameter giving $\kappa = 0{\cdot}167$, and the O-rings were 6·6 and 9·8 cm in diameter. In doing the theoretical predictions for this experiment, the disk was assumed to be transversely pinned at each O-ring and free at the inner and outer radius. For this configuration, the optimum centripetal tensioning occurs with $m \approx 5{\cdot}5$.

For each set of wedges, the disk was spun at speeds ranging from 0 to 2400 r.p.m. The disk was excited manually by lightly striking it with a steel hammer and its transverse displacement was measured using a Philtec photonic sensor with a sensitivity of $1{\cdot}0 \times 10^{-4}$ m/V. The autospectrums of the vibration signal between 0 and 150 Hz were measured three times using eight averages, and then each of these three results were averaged.

The measured and predicted natural frequencies for $m = 0$, 1·4, 2·0 and 5·5 are shown in Figure 11. Overall there is excellent agreement between the measurements and the theoretical predictions. This is particularly true for the lowest natural frequencies, which are the crucial ones in this experiment. The predicted and measured critical speeds for each disk are shown in Table 2. In these experiments, the measurements were stopped at 2400 r.p.m. because of an aerodynamic instability of the disk. This aerodynamic instability occurs at the speed expected from other experimental studies [19] and is unrelated to the effectiveness of centripetal tensioning. Consequently, for the case of $m = 5{\cdot}5$ which has a critical speed greater than 2400 r.p.m., it was not possible to measure the critical speed. However, the agreement of the lowest frequencies between the experimental and theoretical results up to 2400 r.p.m. is excellent.

For the other values of m, there is excellent agreement between the predicted and measured critical speeds, with errors less than 4%. These results corroborate the theoretical predictions and modelling done by Renshaw [7] and confirm that a six-wedge design does not suffer any asymmetric degradation.

There are, however, more vibration frequencies on these curves than predicted by the axisymmetric analysis. Some frequencies appear to have been split due to asymmetry and show two separate sets of frequency measurements following a single analytical prediction. In other cases, frequency deviations may result from effects such as aerodynamic coupling, coupling between the disk and the wedges, and asymmetry of the disk (including runout, residual stresses and warping). For example, in Figure 11(d), there are a number of measured frequencies between 40 and 50 Hz for rotation speeds above 2000 r.p.m. This is just before aerodynamic instability occurs, and one can guess that aerodynamic forces may be responsible in part for these frequencies. While some frequency deviations could perhaps be identified with more sophisticated analyses, this has not been attempted here.

5. CONCLUSIONS

The effect of asymmetry on centripetal tensioning of high speed rotating disks has been studied using the finite element method. The principal findings of this analysis are as follows. (1) A minimum of five concentrated point loads distributed along the inner edge of a rotating disk are as effective as an equipollent, uniformly distributed load for centripetal tensioning. Four or fewer concentrated loads produce degraded tensioning results due to asymmetry of the tensioning stresses. (2) In performing finite element analysis of a rotating circular disk, symmetric finite element meshes should be used to avoid spurious frequency results that can occur using asymmetric meshes. (3) Experimental results using a six-wedge centripetal tensioning design corroborate both the theoretical predictions of centripetal tensioning modelling and the design rules developed here.

REFERENCES

1. D. S. Dugdale 1963 *International Journal of Engineering Sciences* **1**, 89–100. Effect of internal stress on the flexural stiffness of discs.
2. C. D. Mote, Jr. 1965 *Journal of Engineering for Industry* **87**, 285–264. Free vibration of initially stressed circular disks.
3. D. S. Dugdale 1966 *International Journal of Production Research* **4**, 237–248. Theory of circular saw tensioning.
4. C. D. Mote Jr. and L. T. Nieh 1973 *Wood Fiber* **5**, 160–169. On the foundations of circular-saw stability theory.
5. J. F. Carlin, F. C. Appl, H. C. Bridwell and R. P. DuBois 1975 *Journal of Engineering for Industry* **97**, 37–48. Effects of tensioning on buckling and vibration of circular saw blades.
6. G. S. Schajer and C. D. Mote, Jr. 1983 *Wood Science and Technology* **17**, 287–302. Analysis of roll tensioning and its influence on circular saw stability.
7. A. A. Renshaw 1998 *Journal of Sound and Vibration* **210**, 431–439. Increasing the maximum stable rotation speed of a circular disk using speed dependent clamping.

8. C. D. MOTE, JR. 1973 *Journal of Dynamic Systems, Measurement, and Control* **94**, 64–70. Stability control analysis of rotating plates by finite element: emphasis on slots and holes.
9. R. G. PARKER and C. D. MOTE, JR. 1991 *Journal of Sound and Vibration* **145**, 95–110. Tuning of the natural frequency spectrum of a circular plate by in-plane stress.
10. R. C. YU and C. D. MOTE, JR. 1987 *Journal of Sound and Vibration* **199**, 409–427. Vibration and parametric excitation in asymmetric circular plates under moving loads.
11. I. Y. SHEN and C. D. MOTE, JR. 1991 *Journal of Sound and Vibration* **149**, 164–169. Parametric resonances of a circular plate with inlcusions subjected to a rotating spring.
12. I. Y. SHEN and C. D. MOTE, JR. 1992 *Journal of the Acoustical Society of America* **91**, 1489–1499. Dynamic analysis of three-dimensional, finite, linear, elastic solids with Kelvin viscoelastic inclusions: theory with applications to asymmetrically damped circular plates.
13. I. Y. SHEN and C. D. MOTE, JR. 1992 *Journal of Sound and Vibration* **155**, 443–466. Dynamic analysis of three-dimensional, finite, linear, elastic solids containing small elastic imperfections: theory with applications to asymmetric circular plates.
14. J. S. CHEN and J. L. JHU 1997 *Journal of Applied Mechanics* **64**, 897–904. In-plane stress and displacement distributions in a spinning annular disk under stationary edge loads.
15. J. L. NOWINSKI 1964 *Journal of Applied Mechanics* **31**, 72–78. Nonlinear transverse vibrations of a spinning disk.
16. C. D'ANGELO III and C. D. MOTE, JR. 1993 *Journal of Sound and vibration* **168**, 1–14. Natural frequencies of a thin disk, clamped by thick collars with friction at the contacting surfaces, spinning at high rotation speed.
17. W. D. IWAN and T. L. MOELLER 1976 *Journal of Applied Mechanics* **43**, 485–490. The stability of a spinning elastic disk with a transverse load system.
18. N. C. PERKINS and C. D. MOTE, JR. 1986 *Journal of Sound and Vibration* **106**, 451–463. Comments on curve veering in eigenvalue problems.
19. A. A. RENSHAW, C. D'ANGELO III and C. D. MOTE, JR. 1994 *Journal of Sound and Vibration* **177**, 577–590. Aerodynamically excited vibration of a rotating disk.